Inverse Estimation of the Flow Resistivity Tensor of Open-Cell Foams from Experimental Data and Darcy's Flow Simulations

Christophe Van der Kelen*, Peter Göransson, Nils-Erik Hörlin
Marcus Wallenberg Laboratory for sound and vibration research, KTH Aeronautical and Vehicle Engineering, SE -10044 Stockholm
*Corresponding author: Teknikringen 8, SE -11428 Stockholm, cjfvdk@kth.se

Abstract: The flow resistivity tensor, which is the inverse of the viscous permeability tensor, is one of the most important material properties for the acoustic performance of open cell foams, used in acoustic treatments. Due to the manufacturing processes, these foams are most often geometrically anisotropic. This paper discusses the estimation of the flow resistivity tensor using an improvement of a previously published method by Göransson, Guastavino et al. First, flow measurements were performed for different orientations of a cubic porous sample. The modelling of the flow resistivity tensor is centred around a three-dimensional Darcy's law model in COMSOL Earth Science Module, representing the experimental set up. The simulations are performed within an optimisation loop, to determine which flow resistivity tensor gives the best fit of the simulation results to the experimental data, of volume flow and pressure drop between the inlets and outlets. The discussion focuses on the optimiser, the use of COMSOL Multiphysics and the identified flow resistivity tensor of a Melamine sample.

Keywords: Flow resistivity, Melamine, anisotropic, porous, pressure

1. Introduction

Porous materials, such as foamed polymers or fibrous wools, used in vibro-acoustic applications are commonly assumed to behave isotropically in terms of elastic and acoustic properties. However, due to manufacturing processes, porous materials often have an anisotropic geometry. For fibrous wools, the degree of anisotropy is linked to the layering of the fibres and the subsequent compression to desired thickness and density. Commonly they are considered to be transversely isotropic. For foamed materials, the anisotropy is related to the influence of gravity during expansion, in combination with the placement of the injection nozzles, depending on the manufacturing method used. For these materials, the degree of anisotropy is higher.

A new methodology was proposed by by Göransson, Guastavino et al.[1] to estimate the full, anisotropic flow resistivity tensor for a porous material. The method was verified for an ideal theoretical transversely isotropic material, but the application range can be extended to orthotropic materials. The current paper verifies the validity of this extension, and expands the method with the optimisation algorithm Globally Converging Method of Moving Assymptotes[2] (GCMMA) to assure that the solution converges. The GCMMA optimiser is in several ways a considerable improvement compared to the previously used Method of Moving Asymptotes[3] (MMA), as discussed in the paper.

The paper begins with a review of the experimental set up, and then discusses the model, used to simulate the anisotropic flow resistivity. The method is verified for different cases of anisotropic flow resistivity tensors, and compares the MMA and GCMMA optimisers. The paper concludes with a discussion on the modelling in COMSOL, and presents the identified flow resistivity tensor for a Melamine sample, applying the presented method.

2. Experimental set up

The experiments are performed with a symmetric cubic set up which is a generalisation of the standardised static 'flow - pressure drop' measurement[4]. Figure 1 gives a graphical presentation of the set up[1]. The most important features are repeated here, for the sake of completeness.

- The sample is placed in an airtight cubic box built out of aluminium plates with an inner length dimension of 99 mm, and circular openings of 42 mm diameter on each face.

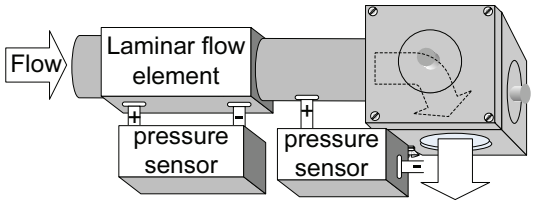

Figure 1. General arrangement of flow and pressure sensors in the measurement set up.

- The flow velocity at the inflow orifice is measured simultaneously with the pressure difference between inlet and outlet openings.

The flow passes through a calibrated laminar element, allowing the flow rate to be estimated before it enters the sample, with the help of a pressure sensor. The pressure drop between the in- and out- flow directions of the sample is estimated with a differential pressure transmitter.

The openings on each face can be either sealed with a plug or connected to a pipe with flow. The flow may be directed from one opening on one face to an opening on any of the other faces, by inserting or removing the plugs, which allows recording the corresponding pressures and velocities.

Five data sets are recorded per inflow face, i.e. the inward flow and the corresponding pressure drops along the 5 possible outflow faces. 30 Pairs of data are recorded, from which 15 are independent because of the theoretically required symmetry of the measurement and the associated reciprocity of the flow resistivity tensor. The remaining measured data are used for quality control checks. A measurement is not accepted if the deviation between reciprocal directions is larger than 5 percent.

These 15 pressure differences of all possible inlet-outlet combinations are required to visualise the 3D flow field in the material and to obtain the 6 unknowns in the flow resistivity tensor.

3. Inverse estimation

The inverse modelling of the flow resistivity tensor is done by calculating the pressure differences over the sample. These pressure differences are solutions from a three-dimensional Darcy's law model in COMSOL Earth Science Module[5], representing the experimental set up. The cost function for the optimiser is defined as the sum of the squares of the relative differences between the measured and the computed pressure differences.

3.1 Governing equations

The intended modelling context, in which the estimated flow resistivity will be used, is the linear acoustic approximation in the frame of Biot models[6], in which the physics on micro scale are homogenised to macro scale, where the fluid is assumed to be inviscid. This is also valid for Darcy's law[7], where the static flow resistivity accounts for the viscous effects at micro scale, and justifies the assumption that the static fluid flow in the porous medium is governed by Darcy's law, i.e. neglecting viscosity on macro scale, and inertial effects in the flow.

The flow inside the porous domain is then determined by the second order permeability tensor $\boldsymbol{\kappa}$, the dynamic viscosity η, the pressure p and the volume average velocity $\mathbf{v} = \{v_x, v_y, v_z\}$ together with a proper set of boundary conditions.

Darcy's law states that

$$-\frac{\boldsymbol{\kappa}}{\eta}\nabla p = \mathbf{v} \quad , \tag{1}$$

which together with an assumed incompressibility condition

$$\nabla \cdot \mathbf{v} = 0 \tag{2}$$

gives

$$\nabla\left(\frac{\boldsymbol{\kappa}}{\eta}\nabla p\right) = 0 \quad . \tag{3}$$

Rewriting Eq. (3) in terms of the second-order flow resistivity tensor $\boldsymbol{\sigma}$ gives

$$\nabla\left(\boldsymbol{\sigma}^{-1}\nabla p\right) = 0 \tag{4}$$

with boundary conditions

$$\nabla p \cdot \mathbf{n}_i = \bar{\sigma}\bar{\mathbf{v}} \cdot \mathbf{n}_i, \mathbf{x} \in \mathbf{X}_i^{\text{in-flow}}, i = 1,...,6 \quad (5)$$

$$\nabla p \cdot \mathbf{n} = 0, \quad \mathbf{x} \in \mathbf{X}^{\text{rigid walls}} \quad (6)$$

$$p = 0, \mathbf{x} \in \mathbf{X}_j^{\text{out-flow}}, j = 1,...,6 \quad i \neq j \,. \quad (7)$$

The indices *i* and *j* refer to the faces of the cubic sample. $\mathbf{x} = \{\mathbf{x}, \mathbf{y}, \mathbf{z}\}$ is the location vector, $\mathbf{X}^{\text{inflow}}$ and $\mathbf{X}^{\text{outflow}}$ are the inflow and the outflow boundaries respectively, $\mathbf{n}$ is the normal vector pointing outwards from the domain, $\bar{\mathbf{v}}$ is the prescribed inflow velocity at an open boundary, and $\bar{\sigma}$ is a flow resistivity to be determined.

3.2 Properties of the flow resistivity tensor

Several properties of the flow resistivity tensor are useful in the estimation process. By definition $\boldsymbol{\sigma}$ is positive definite and symmetric[1]. In addition, the variation over space of the flow resistivity is assumed to be small over the scale of the sample size. The material can then be considered as homogeneous.

3.3 Modelling using COMSOL Multiphysics

A numerical model of the experimental set up predicts the pressure differences over the porous material, as a function of the flow resistivity tensor that is given by the optimisation. This numerical model is developed with the three-dimensional Darcy's law application in COMSOL Earth Science Module.

The boundary conditions related to the flow into the porous medium are an important aspect of the modelling. Two options are possible: either the measured pressure differences or the known flow velocity at the inlet can be chosen as boundary condition to the problem. Then the other quantity is calculated and serves as input for the optimisation. Both possibilities were evaluated in the course of the development, and the measured static flow velocities are selected as boundary condition since the calculated pressure differences served as better input for the optimisation loop, mainly due to scaling of the parameters.

The actual inlet flow velocity through the cubic device in the experiment is calculated from the pressure drop over the laminar flow element.

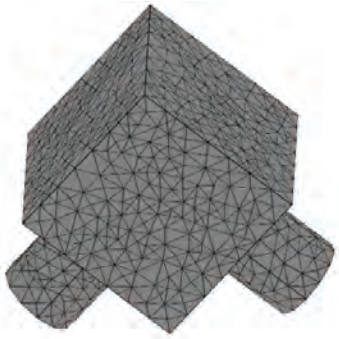

Figure 2. Finite element mesh for cube with tube fittings.

Cylindrical tubes connect the laminar flow element to the cubic sample holder. The flow profile, which is the input in the prediction, is assumed to be uniform over the cross section of the cylindrical tubes, at a certain distance away from the inlet to the cubic measurement device.

In order to approximate the measurement set up in the best way possible, the model is fitted with cylindrical tube-like extensions, similar to the ones used in the experiments, to properly define the boundary conditions for both pressure and flow field, figure 2. To ensure a flow in these tubes, which would not influence the results from the simulations, an isotropic flow resistivity $\bar{\sigma}$ was introduced, see eq. (5); this isotropic flow resistivity in the tubes is five orders of magnitude lower than the flow resistivity in the porous medium under inspection.

By choosing the inlet flow velocity as a boundary condition, the pressure differences between inflow and outflow openings must be calculated from the solution of Eq. (1), as functions of the unknown flow resistivity tensor, together with the boundary conditions in Eqs. (5)- (7).

Since the governing equation for the problem is Darcy's law, the COMSOL Multiphysics package, Earth science module is used to model the porous material inside the cubic sample holder, and to calculate the pressure differences between inlet and outlet. The flow resistivity tensor, which is the outcome of the optimisation, represents the porous material inside the cubic space and the tube fittings adopted. For each of

the 15 inflow-outflow combinations, one model of the order of 20000 degrees of freedom is created, using quadratic order Lagrange polynomial tetrahedral elements, and calculates the pressure differences for a given flow resistivity tensor. These 15 values are then compared to the measured data.

3.4 Inverse estimation procedure

The flow resistivity tensor was estimated such that the sum of the squares of the relative differences between the measured and the computed differential pressures is minimised, with the positive definiteness of $\boldsymbol{\sigma}$ as a side condition to avoid non-admissible solutions.

The cost function[1]

$$\min \sum_{ij} \varepsilon_{ij}^2 \tag{8}$$

is minimised, where

$$\varepsilon_{ij}(\boldsymbol{\sigma}) = \frac{\left(\frac{1}{2}\left(p_{ij}^{measured} + p_{ji}^{measured}\right) - p_{ij}^{computed}(\boldsymbol{\sigma})\right)}{\frac{1}{2}\left(p_{ij}^{measured} + p_{ji}^{measured}\right)} \tag{9}$$

The results in the current paper are obtained using the optimisation algorithm Globally Converging Method of the Moving Asymptotes by Svanberg[2] which was used to fit the model to the measured data in the least square sense. This is an important extension and a considerable improvement compared to the method proposed by Göransson, Guastavino et al.[1], which used the Method of Moving Asymptotes[3], as discussed in the following.

4. Results

4.1 Verification of estimation procedure

The computational parts of the simulation are validated by estimating a known flow resistivity tensor. This was done earlier[1], but only for an ideal theoretical transversely isotropic material. The set of randomly chosen validation tensors are positive definite, symmetric and have diagonal values which are in two cases one order of magnitude higher than the off diagonal values, and in the other two cases two orders of magnitude higher. For the validation, the 15 inflow-outflow pressure differences were computed for given static flow velocities, and then re-used as targets in the estimation.

The proposed inverse estimation method has been verified in four cases, the a-priori known tensors for all cases are given here:

$$\text{Case 1: } \begin{bmatrix} 10000 & 3800 & 2800 \\ 3800 & 9800 & 5200 \\ 2800 & 5200 & 12400 \end{bmatrix}$$

$$\text{Case 2: } \begin{bmatrix} 10000 & -3800 & 2800 \\ -3800 & 9800 & -5200 \\ 2800 & -5200 & 12400 \end{bmatrix}$$

$$\text{Case 3: } \begin{bmatrix} 10000 & 380 & 280 \\ 380 & 9800 & 520 \\ 280 & 520 & 12400 \end{bmatrix}$$

$$\text{Case 4: } \begin{bmatrix} 10000 & -380 & 280 \\ -380 & 9800 & -520 \\ 280 & -520 & 12400 \end{bmatrix}$$

There are two cases with higher off diagonal values to test the reach of the optimisation. The other two cases are lower off diagonal values to test if the optimisation is sensitive to these small values.

Table 1 gives the maximum relative errors for the flow resistivity tensor for all cases using both the GCMMA and MMA optimiser. All solutions were calculated with 100 iterations for both GCMMA and MMA.

Table 1: Largest relative error for all 4 verified cases using both optimisers.

Case	GCMMA	MMA
Case 1	0.03 %	0.10 %
Case 2	0.02 %	0.11 %
Case 3	0.03 %	0.03 %
Case 4	0.52 %	0.02 %

The error in case 4 with the GCMMA optimiser is higher than the other errors since the solution was not yet fully converged. In general, the largest relative error appears for the off-diagonal values.

4.2 MMA vs. GCMMA

The GCMMA optimiser has several advantages over the MMA optimiser with regard to this application. Due to an internal control algorithm, every new proposed set of parameters brings the cost function closer to the minimum than the previous set of parameters. This is obvious from figure 3. Whereas for the MMA optimiser the cost function first jumps away from the minimum, and this happens several times before reaching the minimum, the GCMMA optimiser does not show this behaviour. Therefore a first advantage is that GCMMA is less time consuming since it needs less iterations to find the minimum compared to MMA.

A second advantage is that an optimal solution will be obtained, independent of the number of iterations performed. With MMA the solution obtained just before the iteration ended can be a better solution than the final one, but GCMMA avoids this.

A third advantage, having in mind that both MMA and GCMMA sometimes violate the constraint conditions, is that this violation can be corrected with GCMMA, but not with MMA. An example would be that, if the MMA optimiser violates the constraint conditions and results in a negative definite tensor, it is not possible to solve the problem. If GCMMA violates the constraint condition of the problem, it will correct itself. In this sense, by assuring a converged solution of the simulation, GCMMA is an extension of MMA.

To conclude, GCMMA is a more robust method than MMA, and is therefore an improvement in the inverse estimation, as compared to the first attempt in this direction.

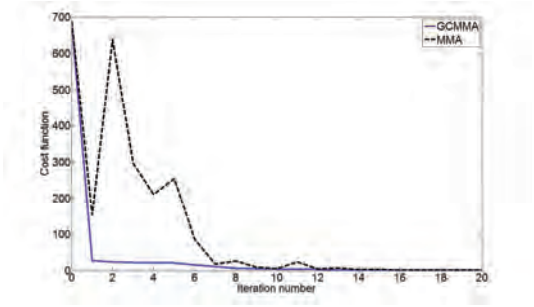

Figure 3. Finite element mesh for cube with tube fittings.

4.3 COMSOL objections

When repeating the computations using the exact same inputs, leaving the inverse estimation unchanged, results have been observed which are different between the two computations. The background of this problem seems to be related to the mesh. The initial mesh is a 'normal' mesh and while solving the problem, one adaptive mesh is necessary to approximate the solution at the sharp edges. This meshing procedure was found to be optimal to avoid corrupted elements in the mesh. The adaptive meshing yields the differences in the simulation results.

An explanation of this phenomenon might be that the adaptive meshing is based on a random algorithm, and thus the mesh might slightly differ in every model, which affects the COMSOL output. The solutions do not differ much, since the GCMMA optimiser tries to obtain the same minimum for the cost function. An algorithm which limits the COMSOL output to 7 significant digits has been successfully implemented as a workaround, to minimize the effect of the random factor in the adaptive meshing.

4.4 Application to a Melamine sample

Following the successful validation of the inverse estimation procedure, the method was applied to a Melamine sample, with mass density 14 kg/m³. This Melamine was grown in one direction, and is expected to show larger flow resistivity in this direction of growth than in the other two directions.

Using the inverse estimation procedure, Eq. (8), and the measured pressure differences over the cubic melamine sample, the flow resistivity tensor shown in Eq. (10) was found[a].

$$\boldsymbol{\sigma} = \begin{bmatrix} 9800 & 3 & -11 \\ 3 & 9700 & 8 \\ -11 & 8 & 10900 \end{bmatrix} \qquad (10)$$

The full anisotropic flow resistivity tensor obviously depends on the orientation of the sample tested and the inherent directivities induced by the manufacturing processes used.

An alternative picture and perhaps also better understanding of the intrinsic flow resistivity of the material may be gained by computing the eigenvalues and eigenvectors of the flow matrices, i.e. through determination of the principal directions and their corresponding principal flow resistivities.

Starting from the identified tensor, Eq. (10), the principal directions for the flow resistivity of the investigated melamine sample were identified in terms of its eigenvalues and eigenvectors. Solving the eigenvalue problem, three distinct principal flow resistivities are obtained, in units (Pa s/m²),

$$\sigma_1 = 10900$$
$$\sigma_2 = 9800$$
$$\sigma_3 = 9700$$

together with three orthogonal, directional eigenvectors[b].

[a] All numerical values presented for the flow resistivities throughout the paper are rounded off to three significant digits.

[b] The eigenvalues and eigenvectors were in all cases throughout the paper computed using the full numerical precision in the flow resistivity tensor, thus a calculation based on the flow resistivity values given in the paper will deviate slightly.

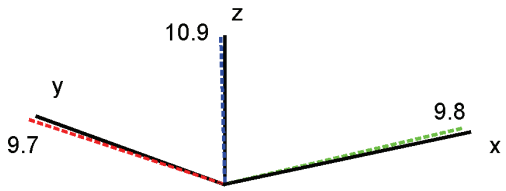

Figure 4. Principal directions for original data shown together with body coordinate system. Indicated are also the flow resistivities in the principal directions in (10^3 Pa s/m^2).

$$\boldsymbol{\Phi}_1 = \{-0.01 \quad 0.01 \quad 0.99\}$$
$$\boldsymbol{\Phi}_2 = \{-0.99 \quad -0.04 \quad -0.01\}$$
$$\boldsymbol{\Phi}_3 = \{-0.04 \quad 0.99 \quad -0.01\}$$

These results clearly show that it is reasonable to assume that Melamine behaves transversely isotropic considering the flow resistivity tensor. A graphical representation of the principal directions is included to provide additional insight into the understanding of the flow resistivity properties of the Melamine, see figure 4. The direction of growth, here z, has a higher flow resistivity than the other material directions, as expected.

5. Conclusions

The method proposed by Göransson, Guastavino et al.[1] has been verified for a wider range of applications. Where before it was only shown that the method works for an ideal theoretical transversely isotropic material, it has now been shown that the method is also valid to find the flow resistivity for orthotropic materials.

Furthermore, using the GCMMA optimiser is an important extension and a considerable improvement to the method. The method is more stable, converged solutions are assured, and are found more quickly.

The effect of the arbitrary factor in the adaptive meshing algorithm of COMSOL has been minimised by limiting the COMSOL output to 7 significant digits. The mesh can in a next step be simplified by replacing the cylindrical

tube-like extensions by square ones, to possibly avoid the problems with COMSOL adaptive meshing. The effect on the mesh and on the solutions of this change to square extensions needs to be investigated.

Finally the full, anisotropic flow resistivity tensor for a sample of Melamine has been identified. Computing the eigenvalues and eigenvectors of the estimated tensors, it was found that the respective flow resistivity tensor is close to transversely isotropic. The direction of highest flow resistivity is aligned with the direction of growth of the Melamine sample.

6. References

1. Peter Göransson, Rémi Guastavino et al, Measurement and inverse estimation of 3D anisotropic flow resistivity for porous materials, *Journal of Sound and Vibration*, **327**, 354-367 (2009)
2. K. Svanberg, A class of globally convergent optimization methods based on conservative convex separable approximations, *SIAM Journal of Optimization*, **12**, 555-573 (2002)
3. K. Svanberg, The method of moving asymptotes - a new method for structural optimization, *International Journal for Numerical Methods in Engineering*, **24**, 359-373 (1987)
4. International Organization for Standardization, Geneva, Switzerland, *Iso 9053:1991:acoustics-material for acoustical application-determination of airflow resistance* (1991)
5. COMSOL Multiphysics 3.5, www.comsol.com
6. M.A. Biot, Theory of propagation of elastic waves in fluid-saturated porous solid. I. Low frequency range, *Journal of the Acoustical Society of America*, **28**, 168-178 (1956)
7. H. Darcy, *Fontaines publiques de la ville de Dijon*, Libraire des Corps. Impériaux des Ponts et Chaussées et des Mines, 1856.

7. Acknowledgements

The authors would like to acknowledge the support from the European Union, the Smart Structures project (Contract no. MRTN-CT-2006-035559) under which the research has been performed. The authors would also like to express their appreciation to Mr Kent Lindgren and Mr Danilo Prevelić for their precious help with the set up and the experiments. We would also like to humbly dedicate this contribution to our late colleague and former teacher Professor Walter Lauriks, KUL, who generously provided us with the Melamine sample tested.

8. Appendix

The principle directions and principal values for all cases stated in section 4.1 are given here.

Case 1:

$$\sigma_1 = 18800$$
$$\sigma_2 = 8200$$
$$\sigma_3 = 5200$$

$$\mathbf{\Phi}_1 = \{0.46 \quad 0.58 \quad 0.67\}$$
$$\mathbf{\Phi}_2 = \{-0.80 \quad -0.06 \quad 0.60\}$$
$$\mathbf{\Phi}_3 = \{-.39 \quad 0.81 \quad -0.44\}$$

Case 2:

$$\sigma_1 = 18800$$
$$\sigma_2 = 8200$$
$$\sigma_3 = 5200$$

$$\mathbf{\Phi}_1 = \{0.46 \quad -0.58 \quad 0.67\}$$
$$\mathbf{\Phi}_2 = \{-0.80 \quad 0.06 \quad 0.60\}$$
$$\mathbf{\Phi}_3 = \{0.39 \quad 0.81 \quad 0.44\}$$

Case 3:

$$\sigma_1 = 12500$$
$$\sigma_2 = 10200$$
$$\sigma_3 = 9500$$

$$\mathbf{\Phi}_1 = \{0.14 \quad 0.20 \quad 0.97\}$$
$$\mathbf{\Phi}_2 = \{0.82 \quad 0.53 \quad -0.23\}$$
$$\mathbf{\Phi}_3 = \{0.56 \quad -0.83 \quad 0.09\}$$

Case 4:

$$\sigma_1 = 12500$$
$$\sigma_2 = 10200$$
$$\sigma_3 = 9500$$

$$\mathbf{\Phi}_1 = \{0.14 \quad -0.20 \quad 0.97\}$$
$$\mathbf{\Phi}_2 = \{-0.82 \quad 0.53 \quad 0.23\}$$
$$\mathbf{\Phi}_3 = \{0.56 \quad 0.83 \quad 0.09\}$$